Published in Journal of Applied Physics 96, issue 12, 6966-6969, 2004
which should be used for any reference to this work

Characterization of photonic crystal waveguides based on Fabry-Pérot interference

Iwan Märki, Martin Salt, Ross Stanley,[a] Urs Staufer, and Hans-Peter Herzig
Institute of Microtechnology, University of Neuchâtel, Rue A.-L. Breguet 2, CH-2000 Neuchâtel, Switzerland

We present two methods based on the analysis of Fabry-Pérot interference for a detailed characterization of a 90° corner in a two-dimensional photonic crystal waveguide fabricated in a thin Si membrane. These methods are a means of identifying the critical waveguide elements in the process of improving photonic crystal devices. The effects of the elements forming the photonic crystal waveguide are identified and quantified by means of a stage-by-stage analysis. By Fourier transforming the transmission spectra we observe the amount of light that is back reflected inside the waveguide and based on the fringe contrast of the Fabry-Pérot modulation we calculate the loss contribution of each waveguide element, such as the tapers and the 90° corner.

I. INTRODUCTION

Photonic crystals are periodic structures that provide a great potential for controlling the propagation of light and permit further miniaturization of optical devices.[1–10] Waveguides and waveguide bends can be created for frequencies inside the photonic band gap by introducing line defects into the photonic crystal structure.[11–16] A sharp bend in a photonic crystal, potentially a key component for integrated photonic circuits, provides an opportunity to study the optical characteristics of photonic band gap structures. In this paper, we present two methods based on the Fabry-Pérot interference technique[17] for a detailed and stage-by-stage experimental analysis of light propagation around a 90° bend in a photonic crystal slab. Transmission spectra of samples with different designs are compared for a better understanding of the transmission efficiency. This analysis allows the study of the effects induced by the different elements of the photonic crystal waveguide. By performing a Fourier transform on the transmission spectra, regions in the waveguide where reflections occur are identified. The losses in all the waveguides are evaluated by calculating the loss coefficient, a very important parameter.

The photonic crystal consists of a square array of cylindrical air holes in a thin Silicon membrane surrounded by air (Fig. 1). The structure is designed to give rise to a TE-like (in-plane polarization) photonic band gap around $\lambda \approx 1.5\ \mu$m. The design parameters of the photonic crystal structure are the lattice constant $a=496$ nm, the hole radius $r=190$ nm, and the slab thickness $t=290$ nm. Measurements are performed with an optical setup that includes a tunable laser source ranging from 1440 to 1580 nm.

II. TRANSMISSION EFFICIENCY

In order to study the effects induced by the taper, the ridge waveguide to photonic crystal waveguide interface, and the photonic crystal sections, we fabricated a series of samples that represent the different subelements of a final photonic crystal bend sample. This allows a better understanding of how each element contributes to the final photonic crystal bend spectrum. The first design is a straight multimode waveguide [Fig. 2(a)] on a SiO_2 substrate with a width of 10 μm, a thickness of 290 nm, and an overall length of 2 mm. It serves as reference for the computation of the transmission efficiency.[12] The second design is a straight waveguide with a taper [Fig. 2(b)] that reduces the width to 500 nm, a ridge waveguide section of a length of 25 μm in the middle, and again a taper to increase the width to 10 μm. The length of the two tapers is 75 μm each. The 25 μm middle waveguide section is a free-standing membrane and its width (500 nm) is approximately equal to the width of the photonic crystal waveguide defect channel ($a=496$ nm). This second design allows us to observe the influence of the taper-induced modal conversion. The next stage is the insertion of the photonic crystal containing a straight single line defect (no holes) into the middle of the waveguide [Fig. 2(c)]. The photonic crystal section is a free-standing mem-

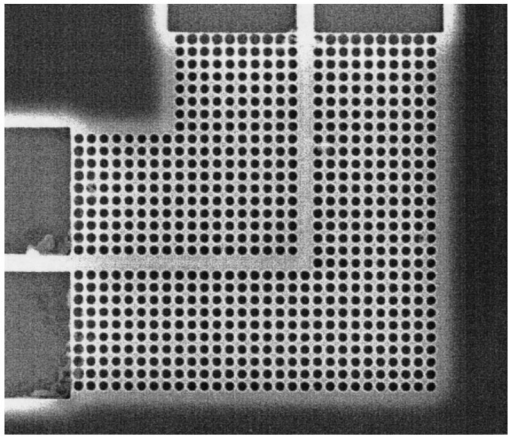

FIG. 1. Scanning electron microscope image of the 90° bend photonic crystal waveguide.

[a]Present address: CSEM, Centre Suisse d'Electronique et de Microtechnique SA, Rue Jaquet-Droz 1, CH-2007 Neuchâtel.

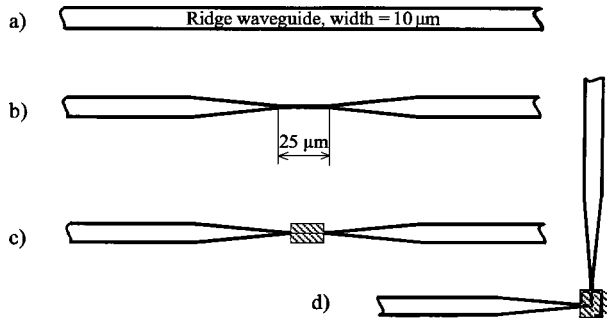

FIG. 2. Designs of the fabricated waveguides: (a) straight waveguide (width=10 μm); (b) straight waveguide with taper and narrow width section (width=500 nm); (c) straight waveguide with photonic crystal waveguide (photonic crystal waveguide length=25 μm); and (d) waveguide with 90° bend.

brane and has a length of 20 μm. It allows us to study the effect of the modal mismatch between the ridge waveguide and the photonic crystal waveguide,[18,19] as well as losses created by the crystal. Finally, the 90° bend is introduced into the photonic crystal waveguide section [Fig. 2(d)].

III. REFLECTIONS AND LOSS CALCULATIONS

All the measured transmission spectra of the different waveguide types exhibit a characteristic Fabry-Perot interference pattern (shown in the inset of Fig. 3), which is mostly due to the smooth end facets and which will be discussed in detail in the following section. To obtain the approximate transmission efficiency of the different waveguides, shown in Fig. 3, we first remove numerically the periodic Fabry-Perot interference pattern and secondly, we divide the transmission spectra by the spectrum of the straight reference waveguide for normalization. This eliminates extrinsic effects of the end injection and most of the spectral response of the measurement optics. Repeated transmission measurements have confirmed that the experimental setup is sufficiently stable to validate the used normalization method. The remaining error is therefore due to fabrication-induced variations between the different waveguides. A transmission efficiency of nearly 85% (±10%), which includes ridge waveguide to photonic crystal losses, is observed for the 90° bend waveguide at a frequency of 1.957×10^{14} Hz. It has a bandwidth of $\Delta f \approx 2700$ GHz for a transmission efficiency of more than 60%. The measured transmission efficiency compares relatively well to the general shape and values of the three-dimensional (3D) simulations, which have been presented in Ref. 19. A detailed modal analysis of the different waveguide types is also presented in Ref. 19.

All back reflections in the waveguide introduce a spectral Fabry-Perot interference pattern related to the path length between reflecting points. Thus, the Fourier transform of the transmission spectra allows the identification of the points where reflections occur.[20] Figure 4 shows the Fourier transform of the different waveguides, which all indicate a dominating Fabry-Perot interference. This dominant peak corresponds to a silicon path length of about 2 mm, and therefore is the Fabry-Perot effect created by the end facets. Our three-dimensional simulations[21] have shown that about 38% of the light is reflected at the silicon/air interface of each end face.

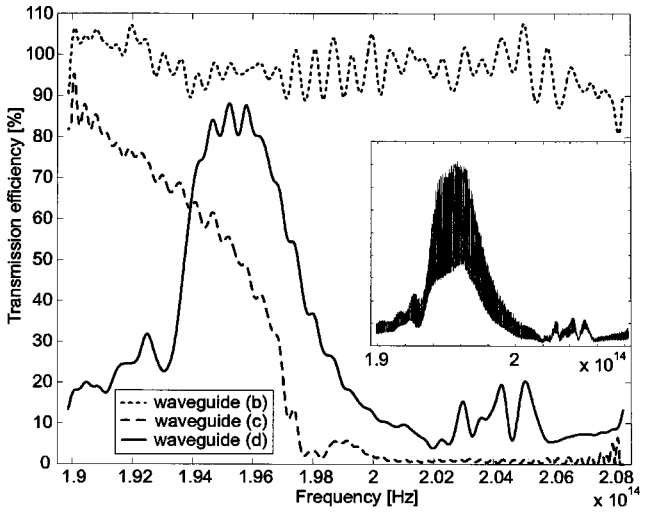

FIG. 3. Transmission efficiency calculated from the measured transmission spectra in reference to the ridge waveguide with a width of 10 μm. The rapid fluctuations are due to interference in the optical system that has not been eliminated in the filtering and normalizing process. The Fabry-Perot interference pattern corresponding to the total length of the waveguide is shown in the inset. The key corresponds to the different waveguide types shown in Fig. 2. The straight waveguide with the tapered section [waveguide (b)] exhibits a relatively flat transmission spectrum. The straight photonic crystal waveguide [waveguide (c)] exhibits a characteristic cutoff which corresponds to the mini stopped band edge. The corner waveguide [waveguide (d)] shows a transmission band with a bandwidth of 2.7 Mhz for a transmission efficiency of more than 60%.

For the design containing the straight photonic crystal waveguide section [Fig. 4(c)], a small second Fabry-Pérot interference appears, which is attributed to the waveguide half length (1 mm) less half the length of the photonic crystal section (10 μm), i.e., ≈1 mm. This suggests the presence of some reflection at the interface between the ridge waveguide and the photonic crystal waveguide section. The much smaller height of the second Fabry-Pérot interference peak in comparison to the first Fabry-Pérot interference peak indicates that the reflection at the interface between the ridge waveguide and the photonic crystal waveguide section is much smaller than the reflection at the end facets (38%). The quantification of the second reflection from the relation between the height of the Fabry-Pérot interference peaks is difficult due to too many unknown parameters such as scattering and radiation. However, our three-dimensional numerical simulations have shown a reflection of 1%–5% at the interface between the ridge waveguide and the photonic crystal waveguide section. Therefore, we can conclude that in the high transmission efficiency range the coupling between the ridge waveguide and the photonic crystal waveguide is quite efficient. In the case of the 90° bend waveguide the secondary Fabry-Pérot interference generated by the Fourier transform over the whole transmission spectrum is about three times as strong as for the straight photonic crystal waveguide. This indicates backreflections at the corner added to the previously observed reflection at the interface between the ridge waveguide and the photonic crystal waveguide. The difference in the path length of the reflection at the waveguide to photonic crystal interface and the reflection at the corner is too small to distinguish the two different peaks in

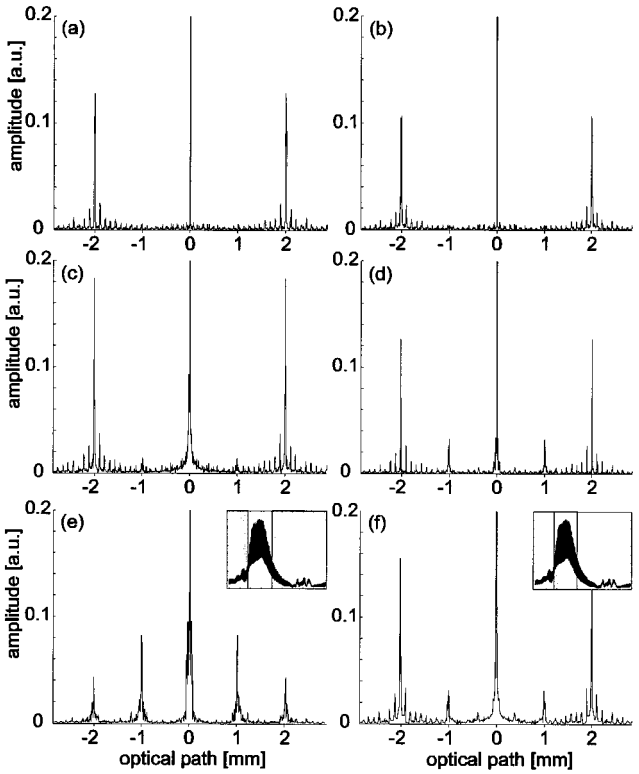

FIG. 4. Fourier transform of the measurement data from the different waveguides: (a) straight waveguide; (b) straight waveguide with taper and narrow section; (c) straight waveguide with photonic crystal waveguide; (d) waveguide with 90° bend; (e) waveguide with 90° bend for frequency ranges where the transmission efficiency is low (indicated dark region in the inset); (f) waveguide with 90° bend for frequency ranges where the transmission efficiency is high (indicated dark region in the inset).

the Fourier transform. At most one can observe a slight broadening of the peak corresponding to the path length of about the half length of the waveguide. For a detailed understanding of these backreflections at the corner, we divide the transmission spectrum into different sections and take the Fourier transform thereof [shown in Figs. 4(e) and 4(f)]. On the one hand, we observe that, for frequency ranges where the transmission efficiency is low, the Fabry-Pérot peak corresponding to the backreflection at the corner is greater than the peak corresponding to the end-facet reflection. In this case, most of the light is reflected at the corner. On the other hand, for the frequency range where the transmission efficiency is high, the backreflection at the corner is low and most of the light travels around the corner. The numerically calculated backreflection at the corner in the case of high transmission is about 1%–5%. In the case of low transmission about 50%–72% of the light is reflected at the corner, depending on the amount of light that is scattered out of the photonic crystal waveguide.

Additional information can be taken from the fringe contrast of the Fabry-Perot modulation in the measured transmission spectrum. Based on the fringe contrast, it is possible to evaluate the losses in the waveguide. Considering our waveguides as simple resonators with losses, we introduce the round-trip intensity attenuation factor,[22] which is related to the two mirror reflectivities (end facets) and the absorption coefficient of the medium associated with both optical absorption and radiation loss,

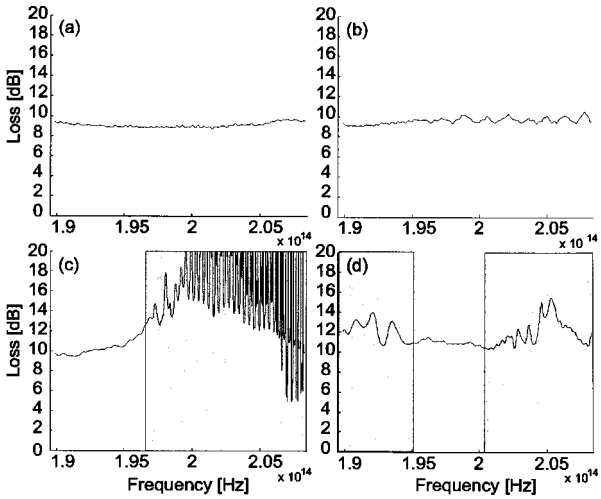

FIG. 5. Calculated overall loss of the different waveguides: (a) simple straight waveguide; (b) straight waveguide with taper and narrow section; (c) straight waveguide with photonic crystal waveguide; (d) waveguide with 90° bend. The gray regions indicate the frequency ranges where the loss calculation is not valid.

$$\mathbf{r}^2 = \mathbf{R}_1\mathbf{R}_2\mathbf{e}^{-2\alpha_s\mathbf{d}}, \tag{1}$$

where R_1 and R_2 represent the end-facet reflectivities, d the total waveguide length of 2 mm, and α_s the absorption coefficient. The maximum and minimum intensity (fringe contrast) observed in the measured transmission spectrum is related to the attenuation factor as follows:

$$\frac{\mathbf{I}_{\max}}{\mathbf{I}_{\min}} = \frac{(1+\mathbf{r})^2}{(1-\mathbf{r})^2}. \tag{2}$$

Using the two relations, we can solve for the absorption coefficient,

$$\alpha_s = \frac{\ln\left(\dfrac{\sqrt{\mathbf{R}_1\mathbf{R}_2}(\sqrt{\mathbf{I}_{\max}} - \sqrt{\mathbf{I}_{\min}})}{(\sqrt{\mathbf{I}_{\max}} + \sqrt{\mathbf{I}_{\min}})}\right)}{\mathbf{d}}. \tag{3}$$

The loss contribution of each element of the bend waveguide can now be calculated, assuming zero material absorption and that the calculated end-facet reflectivities of 38% are not significantly wavelength dependent in our measurement range. In Fig. 5 we show the calculated overall loss for the different waveguides. The straight reference waveguide shows an overall loss of between 8 and 9 dB for the entire measurement range. Considering the waveguide length of 2 mm, we can estimate a relative loss of 4.5 dB/mm. As already observed from the transmission efficiency, the loss calculation of the waveguide with taper confirms that practically no significant losses are induced by the taper. Compared to the reference waveguide, we can attribute an approximate loss of up to 0.5 dB to the taper. For the straight photonic crystal waveguide we observe in the frequency range below the cutoff between 0.5 and 2.5 dB of loss, which is due to the inserted photonic crystal waveguide section. Above the cutoff frequency the loss explodes and the applied loss calculation method looses its validity. The numerical noise above the cutoff frequency is due to a too small Fabry-Perot fringe contrast. From the calculated loss corresponding

to the photonic crystal waveguide section, we can estimate the relative loss coefficient of the defect guide. The section length of 20 μm leads to a relative loss coefficient of 25–125 dB/mm. Recently loss coefficients of 1 and 2.4 dB/mm have been reported.[23,24] Lower quality of the fabricated photonic crystal structure can explain the higher loss coefficient. In addition, in Ref. 19 we have shown with a detailed modal analysis that the dispersion curve of the propagating defect mode is above the light line, which contributes significantly to the loss coefficient. Finally, the loss that can be attributed to the 90° bend waveguide adds up to between 1 and 2.5 dB in comparison to the reference waveguide for the high transmission frequency range. Comparing the 90° bend waveguide with the straight photonic crystal waveguide, we can estimate a loss of 0.5–2 dB due to the corner itself. It should be noted that the applied loss calculation method is valid only to a limited extent in the case of the 90° bend waveguide. As long as any reflections at points in between the end facets are significantly small in comparison with the end-facet reflection, the loss coefficient can approximately be calculated from the Fabry-Perot fringe contrast. However, in the preceding section we have shown that considerable reflections at the corner occur for frequencies where the transmission efficiency is low. Therefore, in that case the applied loss calculation method is not valid.

IV. CONCLUSION

In summary, we have presented simple methods for a detailed analysis of the light propagation around a 90° bend corner in a photonic crystal slab. The presented measurements show efficient waveguiding around a 90° corner and help to understand better the phenomena present in a waveguide containing a section of photonic crystal. Comparing the transmission spectrum of the different waveguide designs has made it possible to evaluate the influence of the subelements of the corner waveguide. We have shown that nearly 85% transmission efficiency was observed for the 90° bend waveguide. By means of the Fourier transform of the transmission spectra we have identified the points where reflections occur inside the waveguide. Based on the fringe contrast of the measured Fabry-Perot modulation in the transmission spectrum, we have calculated the losses of the waveguides. The loss for the straight photonic crystal waveguide was estimated to be 25 dB/mm in the best case. The corner alone adds an estimated loss of 0.5–2 dB for the frequency range where the transmission efficiency is high. The presented methods for the characterization of the photonic crystal waveguide help identify the critical waveguide elements that need improvement. For example, backreflections can be significantly reduced by introducing tapers for better light coupling. Waveguide sections with high losses need improvement by positioning the dispersion curve of the defect mode under the light line and by reducing the roughness of the sample surface.

ACKNOWLEDGMENTS

The authors acknowledge F. Schädelin, S. Gautsch, and P.-A. Künzi for useful discussions and for fabricating the photonic crystal waveguide samples. This work is funded under a joint projects program between the Swiss Center of Electronics and Microtechnology (CSEM) and the IMT-Uni Neuchâtel.

[1] S. G. Johnson, P. R. Villeneuve, S. Fan, and J. D. Joannopoulos, Phys. Rev. B **62**, 8212 (2000).
[2] M. Lončar, J. Vučković, and A. Scherer, J. Opt. Soc. Am. B **18**, 1362 (2001).
[3] M. D. B. Charlton, M. E. Zoorob, G. J. Parker, M. C. Netti, J. J. Baumberg, S. J. Cox, and H. Kemhadjian, Mater. Sci. Eng., R. **74**, 17 (2000).
[4] S. Y. Lin, E. Chow, S. G. Johnson, and J. D. Joannopoulos, Opt. Lett. **25**, 1297 (2000).
[5] M. Lončar, T. Doll, J. Vučković, and A. Scherer, J. Lightwave Technol. **18**, 1402 (2000).
[6] A. Adibi, Y. Xu, R. K. Lee, A. Yariv, and A. Scherer, J. Lightwave Technol. **18**, 1554 (2000).
[7] M. Lončar, D. Nedeljković, T. P. Pearsall, J. V. Vučković, A. Scherer, S. Kuchinsky, and D. C. Allan, Appl. Phys. Lett. **80**, 1689 (2002).
[8] Y. Désières *et al.*, J. Appl. Phys. **92**, 2227 (2002).
[9] X. Letartre *et al.*, Appl. Phys. Lett. **79**, 2312 (2001).
[10] S. Kuchinsky, D. C. Allan, N. F. Borelli, and J.-C. Cotteverte, Opt. Commun. **175**, 147 (2000).
[11] A. Mekis, J. C. Chen, I. Kurland, S. Fan, P. R. Villeneuve, and J. D. Joannopoulos, Phys. Rev. Lett. **77**, 3787 (1996).
[12] E. Chow, S. Y. Lin, J. R. Wendt, S. G. Johnson, and J. D. Joannopoulos, Opt. Lett. **26**, 286 (2001).
[13] A. Talneau, L. Le Gouezigou, N. Bouadma, M. Kafesaki, C. M. Soukoulis, and M. Agio, Appl. Phys. Lett. **80**, 547 (2002).
[14] M. Tokushima, H. Kosaka, A. Tomita, and H. Yamada, Appl. Phys. Lett. **76**, 952 (2000).
[15] A. Chutinan, M. Okano, and S. Noda, Appl. Phys. Lett. **80**, 1698 (2002).
[16] Y. Sugimoto, N. Ikeda, N. Carlsson, K. Asakawa, N. Kawai, and K. Inoue, J. Appl. Phys. **91**, 3477 (2002).
[17] A. Talneau, M. Mulot, S. Anand, and Ph. Lalanne, Appl. Phys. Lett. **82**, 2577 (2003).
[18] E. Miyai, M. Okano, M. Mochizuki, and S. Noda, Appl. Phys. Lett. **81**, 3729 (2002).
[19] I. Märki, M. Salt, and H. P. Herzig, J. Appl. Phys. **96**, 7 (2004).
[20] A. Talneau, Ph. Lalanne, M. Agio, and C. M. Soukoulis, Opt. Lett. **27**, 1522 (2002).
[21] T. Weiland, Int. J. Numer. Model. **9**, 295 (1996).
[22] B. E. A. Saleh and M. C. Teich, *Fundamentals of Photonics* (Wiley, New York, 1991).
[23] M. Notomi, A. Shinya, S. Mitsugi, E. Kuramochi, and H.-Y. Ryu, Opt. Express **12**, 1551 (2004).
[24] S. McNab, N. Moll, and Y. A. Vlasov, Opt. Express **11**, 2927 (2003).